Nanoconfinement in Slit Pores Enhances Water Self-Dissociation

Daniel Muñoz-Santiburcio* and Dominik Marx
Lehrstuhl für Theoretische Chemie, Ruhr–Universität Bochum, 44780 Bochum, Germany
(Received 16 February 2017; published 31 July 2017)

We investigate the self-dissociation of water that is nanoconfined between the sheets of a realistic layered mineral, FeS mackinawite, as well as between Lennard-Jones walls via *ab initio* simulations. By comparing it with the same reaction in bulk water under various thermodynamic conditions, we show that such strong two-dimensional confinement between hard surfaces greatly enhances the self-dissociation process of water—thus increasing its ionic product K_w due to nanoconfinement. In addition to providing free energies, we analyze in detail the underlying dielectric properties in terms of dipole moment distributions, and thus the polarity of the liquid, as well as local polarization fluctuations as quantified by dielectric tensor profiles perpendicular to the lamella.

DOI: 10.1103/PhysRevLett.119.056002

In recent years, nanoconfined water has received steeply increasing attention due to its very peculiar properties such as its extremely confinement-dependent phase behavior [1,2], almost frictionless flow [3], and distinct dielectric properties [4,5]. Other intensely studied processes in nanoconfined water are proton conduction, ion transport, and molecular separation in water nanochannels hosted by tailored nanostructures [6,7], carbon nanotubes [8–11], graphene layers [12–17], or layered minerals [18,19] in view of their very promising applications in energy storage [20–22] or water purification [12].

Yet, there is much to be understood about the effect of the confinement itself on actual chemical reactions in the aqueous phase. While soft confining media such as micelles have been extensively used for studying chemical reactivity, such environments are vastly different from chemically inert and hard confining media such as nanotubes, graphene, or mineral sheets. Indeed, water in such media deserves special attention, and so far only its effect on the conformational equilibrium of biomolecules has been studied [23,24] while other processes involving the breaking and making of covalent bonds remain largely unexplored.

Moving beyond structure and dynamics, this Letter is devoted to unraveling nanometric confinement effects on the most paradigmatic chemical reaction in aqueous environments, namely, water self-dissociation, using both a realistic model of mineral slit pores, namely, mackinawite FeS sheets, and a schematic hydrophobic confinement modeled by Lennard-Jones walls. In particular, we examine nanoconfined water between mackinawite sheets at so-called hydrothermal vent conditions as part of broad investigations into prebiotic chemistry within the "iron-sulfur world" scenario of the origin of life [25–28].

General properties of such nanoconfined neutral water [29] as well as the structural diffusion of excess protons [18] and proton holes [19] have already been explored, revealing that nanoconfinement greatly conditions in an unexpected way the structural diffusion mechanism of $OH^-(aq)$ but not that of $H^+(aq)$. Most recently, we already found remarkable nanoconfinement effects on several complex chemical reactions [28], in particular regarding the qualitative stabilization of charged and charge-separated species in nanoconfined compared with bulk water. In an effort to understand the underlying physical principles, we systematically investigate herein the fundamental water self-dissociation process and disclose that nanoconfinement significantly enhances this elementary reaction compared with the bulk regime. This finding goes hand in hand with significant changes of the dielectric response tensor of the nanoconfined water lamella, while confinement-induced changes of charge defect structures or water polarity cannot explain the phenomenon.

Computational approach.—Our computational model as well as the *ab initio* molecular dynamics [30] setup for nanoconfined hot-pressurized water between mackinawite sheets (NCW) is the validated "wide pore" approach (see Fig. 1) as used to study neutral [29], acidic [18], and basic [19] nanoconfined water as well as a set of complex reactions leading to prebiotic peptide synthesis [28]; see the Supplemental Material [31] for details, including the additional Refs. [32–47].

Self-dissociation in bulk reference systems.—In order to further validate our computational approach to activation free energies for water dissociation in aqueous environments, we apply it first to study the self-dissociation of H_2O in bulk water at temperatures between 350 and 500 K where experimental data are available at variance with nanoconfinement conditions. The data, see $\Delta F^{\ddagger}_{\mathrm{Sim}}$ in Fig. 2 [being the free energy difference between $n_{\mathrm{H}} \approx 2$ and $n_{\mathrm{H}} \approx 1.1$ in Fig. 3(a) obtained from thermodynamic integration, see Sec. I.C in the Supplemental Material [31]], show that even though the simulations systematically underestimate the free energy barrier in absolute terms, its increase with T is essentially quantitatively reproduced compared with experiment (note that the rate of the dissociation reaction,

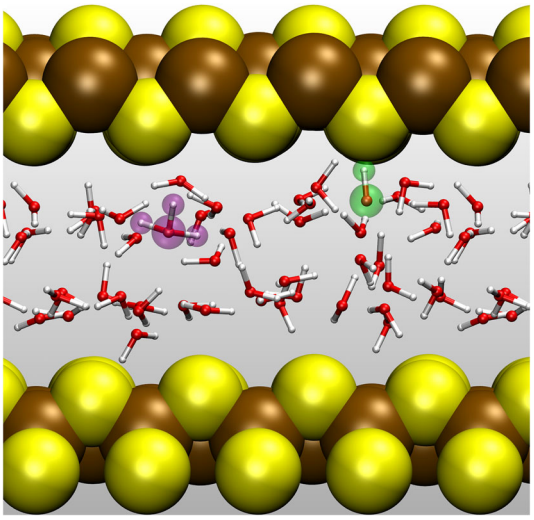

FIG. 1. Representative snapshot of the NCW system that hosts one dissociated water molecule (as obtained from the thermodynamic integration replica with a coordination number of 1.1, see text). Water molecules are shown as red and white balls and sticks whereas the OH^- and H_3O^+ species resulting from the self-dissociation reaction are highlighted with green and purple spheres, respectively, while the Fe and S atoms are shown as brown and yellow spheres.

being roughly $\sim \exp[-\Delta F^{\ddagger}/k_B T]$, increases upon increasing T at constant p). Therefore, our approach is reliable for predicting the change of the dissociation free energy in response to changing conditions. We note that the increase in the energetic cost for water self-dissociation with higher T correlates with a decreasing static dielectric constant of bulk water [48], from $\varepsilon = 62.47$ at 350 K and 20 MPa to 31.25 at 500 K as will be discussed later.

Self-dissociation under confinement.—The free energy profile for water self-dissociation in the NCW system, when compared with those in bulk water at different

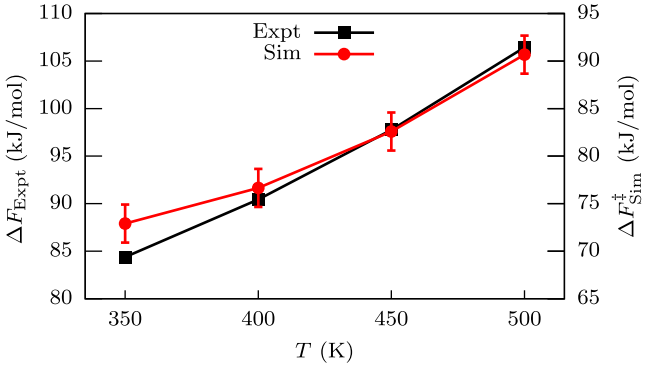

FIG. 2. Activation free energies $\Delta F^{\ddagger}$ for H_2O self-dissociation in bulk water at $p = 20$ MPa as a function of temperature leading to $H^+(aq)$ and $OH^-(aq)$. Note that the scale for the simulation results for $\Delta F^{\ddagger}_{\mathrm{Sim}}$ (with error estimates from Sec. I.D in the Supplemental Material [31]) is shifted upwards for a better comparison with the experimental data for ΔF_{Expt} (obtained from the corresponding experimental [49] ionic products K_w).

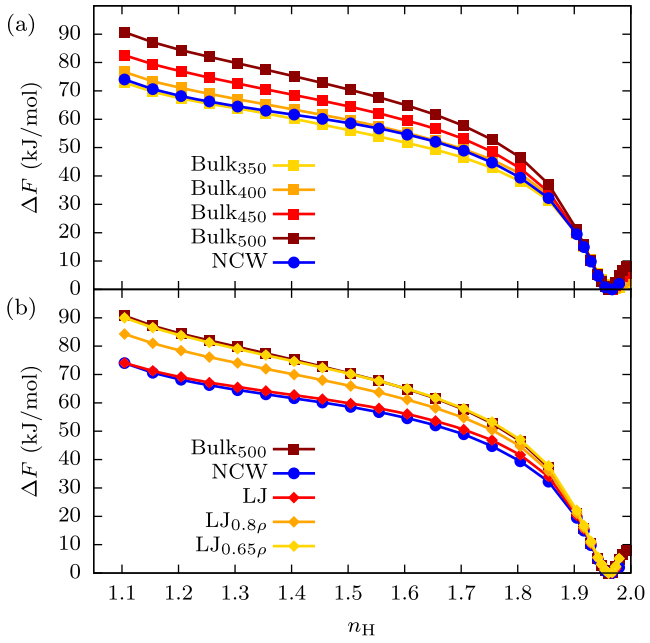

FIG. 3. Relative free energy profiles $\Delta F(n_{\mathrm{H}})$ for the H_2O self-dissociation reaction; $\Delta F^{\ddagger}$ is obtained at $n_{\mathrm{H}} = 1.1$. (a) Bulk water at $p = 20$ MPa and different T versus nanoconfined water within mackinawite sheets (NCW) at $p \approx 20$ MPa and $T = 500$ K. (b) Bulk water at $p = 20$ MPa and $T = 500$ K and nanoconfined water within Lennard-Jones (LJ) walls, which closely reproduces the water density profile of the NCW system, and such systems with average densities reduced to 80% and 65% of the NCW or LJ value ($LJ_{0.8\rho}$ and $LJ_{0.65\rho}$, respectively) compared with NCW conditions (see Sec I.B in the Supplemental Material [31] for definition of the LJ and $Bulk_{500}$ systems).

temperatures [Fig. 3(a)], reveals that the self-dissociation reaction is greatly enhanced by this confinement. Upon changing from the corresponding bulk regime ($p = 20$ MPa, $T = 500$ K) to NCW conditions, the free energy barrier $\Delta F^{\ddagger}$ is reduced by almost the same amount as when reducing T in the bulk regime from 500 K to 350 K. Assuming thermal activation, this corresponds to an acceleration of this chemical reaction by roughly a factor of 55 due to nanoconfinement, which decreases the $pK_w = -\log K_w$ of water by roughly two decadic units.

In previous works [18,19] we found that there are no specific interactions between the FeS sheets and water including $H^+(aq)$ and $OH^-(aq)$, which suggests that the reduced barrier for the self-dissociation reaction discovered here upon nanoconfinement is not a consequence of any specific mineral-water chemistry. In order to confirm that the observed effect is due to the geometric confinement effect as such, we compare the free energy profile in NCW with that obtained for water confined by chemically inert Lennard-Jones (LJ) walls (LJ system, see Sec. I.B in the Supplemental Material [31] for details). It is clearly revealed [Fig. 3(b)] that the reduction of $\Delta F^{\ddagger}$ is due to the confinement itself, since the LJ and NCW profiles overlap almost perfectly.

Dipole distribution of nanoconfined water.—As a first attempt for explaining the remarkable reactivity changes between nanoconfined and bulk water, we investigated the respective H_2O dipole moment distributions (Fig. 4). Importantly, the dipole distributions in the NCW and LJ systems are identical, thus further backing up the conclusion that the behavior of water in FeS sheets is dominated by the confinement itself and not by the distinct chemistry of the interfaces. This holds true upon reducing the water density in the NCW system to 80%, $NCW_{0.8\rho}$, and comparing with the equivalent $LJ_{0.8\rho}$ system. Most importantly, the distributions in the NCW and LJ systems are shifted towards higher dipoles compared with the bulk, while at lower density they are displaced towards smaller dipoles (see the caption of Fig. 4 for the average dipole moments). This makes it unlikely that the different dipole distributions in confinement compared with the bulk are key to understanding the observed changes of $\Delta F^{\ddagger}$: while a more polar solvent could better stabilize charges such as the $H^+(aq)$ and $OH^-(aq)$ species in the case of the NCW or LJ systems, this same argument would not explain why $\Delta F^{\ddagger}$ in the $LJ_{0.8\rho}$ system is still lower than in the bulk despite being "less polar" in that sense, or why $\Delta F^{\ddagger}$ in $LJ_{0.65\rho}$ is almost the same as in the bulk despite its distinctly different dipole distribution. Thus, the altered "polarity" of the liquid (as quantified by its average molecular dipole moment) cannot explain the observed phenomenon.

Solvation structure of $H^+(aq)$ *and* $OH^-(aq)$.—In an effort to possibly unveil a structural basis for the nanoconfinement-induced enhancement of water self-dissociation, we analyzed the solvation structure of the products $H^+(aq)$ and $OH^-(aq)$ in nanoconfinement versus the homogeneous bulk. These final states are found to be similar to what is known from the bulk: the excess proton

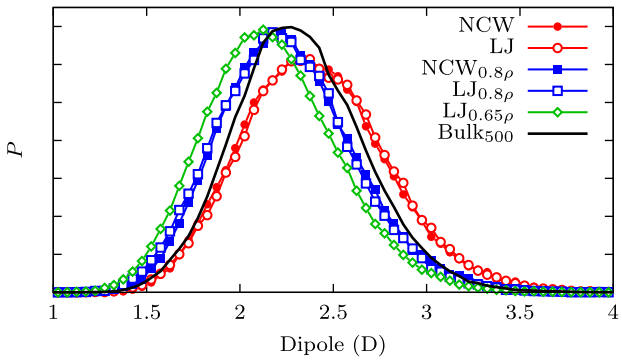

FIG. 4. Normalized distribution functions P of the H_2O dipole moments of nanoconfined water within FeS sheets under NCW conditions and with the density reduced to 80% ($NCW_{0.8\rho}$) compared with nanoconfined water within LJ walls at different densities (LJ, $LJ_{0.8\rho}$ and $LJ_{0.65\rho}$) and with bulk water. The average dipole moments (in D) are 2.40 and 2.41 (for the NCW and LJ systems, respectively), 2.26 and 2.24 ($NCW_{0.8\rho}$ and $LJ_{0.8\rho}$, respectively), 2.17 ($LJ_{0.65\rho}$), and 2.32 ($Bulk_{500}$).

$H^+(aq)$ is properly solvated and diffuses across the whole system via the "Grotthuss mechanism" [50], while the excess hole $OH^-(aq)$ prefers the same "resting state" [50] as demonstrated in Sec. II.B of the Supplemental Material [31]. Moreover, analyzing the solvation structure along the dissociation coordinate (see Sec. II.C of the Supplemental Material [31]), we observe that the initially intact H_2O molecule first generates $OH^-(aq)$ in its proper "active state" before it transmutes to the resting state at full dissociation according to the well-established "dynamical hypercoordination mechanism" [50]. Hence, we conclude that the solvation structure of $H^+(aq)$ and $OH^-(aq)$ in nanoconfinement is the same as in the bulk limit, and, therefore, is not responsible for the observed reduction of the dissociation free energy.

Dielectric profiles of nanoconfined water.—Transcending the analysis of dipole moments and solvation structures, we now investigate their correlations in the sense of spatially resolved dielectric properties quantified in terms of polarization fluctuations. It is well established that the (isotropic) dielectric constant ε (i.e., the relative static permittivity) of bulk water greatly changes with temperature and pressure [51,52]. As we pointed out earlier, the increasing $\Delta F^{\ddagger}$ for water self-dissociation upon increasing T may be explained in terms of the significant decrease of ε: its lower value at high T implies that the charged species formed upon H_2O dissociation are no longer that well stabilized in this dipolar liquid, thus increasing the energetic cost of the process. Now, motivated by recent studies unfolding the surprisingly rich dielectric properties of both interfacial [53,54] and nanoconfined [4,5] water in comparison with the bulk, we set out to compute the (anisotropic) dielectric properties of nanoconfined water within LJ walls. The dielectric tensor for water in planar confinement is diagonal with components $\varepsilon_{\parallel}(z)$ and $\varepsilon_{\perp}(z)$ dependent on the distance z normal to the surface expressed [4] as

$$\varepsilon_{\parallel}(z) = 1 + \frac{c_{\parallel}(z)}{\varepsilon_0 k_B T}, \tag{1}$$

$$\varepsilon_{\perp}^{-1}(z) = 1 - \frac{c_{\perp}(z)}{\varepsilon_0 k_B T + C_{\perp}/V}, \tag{2}$$

where $c_\alpha(z) = \langle m_\alpha(z) M_\alpha \rangle - \langle m_\alpha(z) \rangle \langle M_\alpha \rangle$ and $C_\alpha = A \int_{-L_z/2}^{L_z/2} c_\alpha(z) dz$; here, M_α is the total polarization of the system, L_z the simulation cell length along z, $A = L_x L_y$ is the lateral simulation box area, and $\alpha = \perp, \parallel$. The polarization density $m_{\parallel}(z)$ is computed using only the dipole contributions since higher order multipole moments have been shown to be negligible for the parallel response of interfacial water [53,54], while for the perpendicular profile we integrate the total charge density as $m_{\perp}(z) = -\int_{-L_z/2}^{z} \rho(z') dz'$.

Dielectric properties computed via such polarization fluctuations require long simulations, which are readily

accessible via force field MD. We employed the SPC/Fw water model, which yields excellent ε data of bulk water [55], to compute $\varepsilon_\alpha(z)$ within the nanoconfined water lamella for the different LJ and LJ_ρ systems based on 50 ns *NVT* simulations. Moreover, we performed an NPT run in a 256 bulk water system at 500 K and 20 MPa to demonstrate the excellent agreement of the resulting $\varepsilon_{\mathrm{Sim}} \approx 31$ with experiment [48], $\varepsilon_{\mathrm{Expt}} = 31.25$.

The dielectric profiles of nanoconfined water (Fig. 5) feature significant enhancements of the parallel response $\varepsilon_\parallel$ compared with the isotropic bulk value of ≈31 at 500 K and 20 MPa even in the case of the lamella with the lowest density. Such a striking effect has already been seen at ambient conditions for interfacial water at hard interfaces [53], while for ambient water confined between soft interfaces the effect is much smaller [4]. This enhancement of $\varepsilon_\parallel$ apparently goes hand in hand with the favored self-dissociation of water and thus a greatly enhanced ionic product K_w upon nanoconfinement as found in the reactive *ab initio* molecular dynamics simulations of the LJ systems. On the other hand, the perpendicular response $\varepsilon_\perp$ is far more complex as already revealed for interfacial water in other systems [4,53].

But could it be that what we ascribe to be a "nanoconfinement effect" is merely a "density effect" as a result of overpressurizing water in the slit pore? Therefore, the $LJ_{0.8\rho}$ slit pore model was constructed (see Sec. I.B in the Supplemental Material [31]) to probe the putative scenario that the NCW system could stabilize charged species

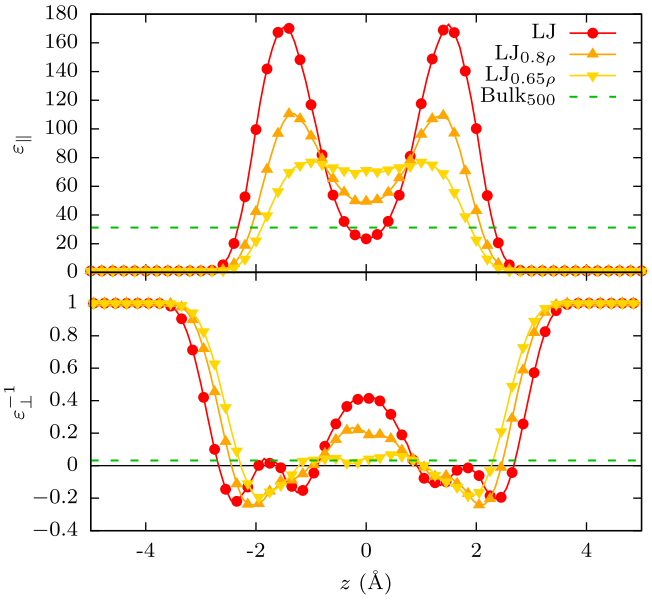

FIG. 5. Parallel ($\varepsilon_\parallel$) and inverse perpendicular ($\varepsilon_\perp^{-1}$) dielectric profiles for nanoconfined water within Lennard-Jones walls with the same density as in the NCW system (LJ) and with the density reduced to 80% and 65% of that value ($LJ_{0.8\rho}$ and $LJ_{0.65\rho}$) compared with ε and ε^{-1} in bulk water.

simply via an increased average water density (which is known to increase the isotropic dielectric constant [48] and to lower the free energy barrier for H_2O dissociation in the homogeneous bulk limit [49]), rather than charge stabilization being a nanoconfinement effect. As shown by Fig. 3, even deliberately decreasing the density by as much as 20% still leads to a lower free energy barrier for the self-dissociation reaction in the nanoconfined $LJ_{0.8\rho}$ system compared with the $Bulk_{500}$ system. Only upon reducing the average density by 35% is a similar free energy barrier provided as the $Bulk_{500}$ system according to the $LJ_{0.65\rho}$ data. Probing the density response supports the finding that the nanoconfinement of water in slit pores is key to lowering the free energy barrier for H_2O self-dissociation.

Last, but not least, we note that the effect disclosed herein is phenomenologically consistent with the results of our recent study of a set of complex chemical reactions in nanoconfined water [28], where we observed stabilization of various charged molecular reaction partners in nanoconfinement compared with the bulk regime.

In conclusion, the water self-dissociation reaction is greatly favored when water is nanoconfined within hard slit pores, such as those offered by layered materials including minerals, compared with the isotropic bulk regime and, therefore, leads to an increased ionic product K_w of water in nanometric spaces. This phenomenon, which we show to be the consequence of nanoconfinement as such, is unrelated to the observed changes of the dipole moment of water molecules and thus is independent of the altered polarity of the liquid in response to confinement. The solvation structures of $H^+(aq)$ and $OH^-(aq)$ under nanoconfinement conditions are moreover found to be very similar to those in the homogeneous bulk environment. In stark contrast, the disclosed effect does correlate with prominent changes of the dielectric response tensor due to nanoconfining water in a slit pore. However, the quantitative relationship between the decrease of the free energy barrier of this self-dissociation reaction, leading to charged species that are solvated in nanoconfined water, and the strongly varying parallel and perpendicular components of the dielectric tensor remains yet to be established. Clearly, future fundamental analytical work is needed in order to work out this link, e.g., by expressing the solvation free energy of charged molecular species in nanoconfined water in terms of the anisotropic polarization fluctuations, akin to what has been achieved recently [56] for simple ions in isotropic bulk water, which might serve as a reference.

Transcending the specific case, it is conceivable that the same effect could be observed in other circumstances where water is confined down to the nanometer scale. Indeed, similar enhancements of the anisotropic dielectric response have already been reported for instance inside carbon nanotubes [57] or cylindrical nanopores [5]. It would not be surprising that this phenomenon can have deep

implications also for technological applications, such as the recently observed unexpected behavior of charge transport and current fluctuations in carbon nanotubes [9]. Apart from that, we expect that nanoconfined dipolar liquids, such as aqueous solutions in the first place, will offer a vast playground for studying and possibly even tuning chemical reactions by purely geometric means.

This work was supported by the German Research Foundation (DFG) via the Cluster of Excellence EXC 1069 "RESOLV." We also acknowledge the Gauss Centre for Supercomputing (GCS) for the computing time provided as a GCS Large Scale Project on the IBM Blue Gene/Q system Juqueen at Jülich Supercomputing Centre as well as HPC@ZEMOS, HPC-RESOLV, and BOVILAB@RUB.

*daniel.munoz@theochem.rub.de

[1] G. Algara-Siller, O. Lehtinen, F. Wang, R. Nair, U. Kaiser, H. Wu, A. Geim, and I. Grigorieva, Nature (London) **519**, 443 (2015).
[2] K. V. Agrawal, S. Shimizu, L. W. Drahushuk, D. Kilcoyne, and M. S. Strano, Nat. Nanotechnol. **12**, 267 (2017).
[3] E. Secchi, S. Marbach, A. Niguès, D. Stein, A. Siria, and L. Bocquet, Nature (London) **537**, 210 (2016).
[4] A. Schlaich, E. W. Knapp, and R. R. Netz, Phys. Rev. Lett. **117**, 048001 (2016).
[5] C. Schaaf and S. Gekle, J. Chem. Phys. **145**, 084901 (2016).
[6] C. Duan and A. Majumdar, Nat. Nanotechnol. **5**, 848 (2010).
[7] S. X. Li, W. Guan, B. Weiner, and M. A. Reed, Nano Lett. **15**, 5046 (2015).
[8] R. H. Tunuguntla, F. I. Allen, K. Kim, A. Belliveau, and A. Noy, Nat. Nanotechnol. **11**, 639 (2016).
[9] E. Secchi, A. Niguès, L. Jubin, A. Siria, and L. Bocquet, Phys. Rev. Lett. **116**, 154501 (2016).
[10] A. Bankura and A. Chandra, J. Phys. Chem. B **116**, 9744 (2012).
[11] S. H. Lee and J. C. Rasaiah, J. Chem. Phys. **139**, 124507 (2013).
[12] S. P. Surwade, S. N. Smirnov, I. V. Vlassiouk, R. R. Unocic, G. M. Veith, S. Dai, and S. M. Mahurin, Nat. Nanotechnol. **10**, 459 (2015).
[13] C. Cheng, G. Jiang, C. J. Garvey, Y. Wang, G. P. Simon, J. Z. Liu, and D. Li, Sci. Adv. **2**, e1501272 (2016).
[14] A. Alhadhrami, S. Salgado, and V. Maheshwari, RSC Adv. **6**, 70012 (2016).
[15] Y. Jiang, P. Biswas, and J. D. Fortner, Environ. Sci.: Water Res. Technol. **2**, 915 (2016).
[16] K. Hatakeyama, M. R. Karim, C. Ogata, H. Tateishi, A. Funatsu, T. Taniguchi, M. Koinuma, S. Hayami, and Y. Matsumoto, Angew. Chem., Int. Ed. Engl. **53**, 6997 (2014).
[17] L. Huang, M. Zhang, C. Li, and G. Shi, J. Phys. Chem. Lett. **6**, 2806 (2015).
[18] D. Muñoz-Santiburcio, C. Wittekindt, and D. Marx, Nat. Commun. **4**, 2349 (2013).
[19] D. Muñoz-Santiburcio and D. Marx, Nat. Commun. **7**, 12625 (2016).
[20] J. Maier, Nat. Mater. **4**, 805 (2005).
[21] S. L. Candelaria, Y. Shao, W. Zhou, X. Li, J. Xiao, J.-G. Zhang, Y. Wang, J. Liu, J. Li, and G. Cao, Nano Energy **1**, 195 (2012).
[22] H. G. Park and Y. Jung, Chem. Soc. Rev. **43**, 565 (2014).
[23] E. J. Sorin and V. S. Pande, J. Am. Chem. Soc. **128**, 6316 (2006).
[24] J. S. Rao, M. D. Smith, and L. Cruz, J. Phys. Chem. B **118**, 3517 (2014).
[25] G. Wächtershäuser, Prog. Biophys. Molec. Biol. **58**, 85 (1992).
[26] C. Huber and G. Wächtershäuser, Science **281**, 670 (1998).
[27] E. Schreiner, N. N. Nair, and D. Marx, J. Am. Chem. Soc. **130**, 2768 (2008).
[28] D. Muñoz-Santiburcio and D. Marx, Chem. Sci. **8**, 3444 (2017).
[29] C. Wittekindt and D. Marx, J. Chem. Phys. **137**, 054710 (2012).
[30] D. Marx and J. Hutter, *Ab Initio Molecular Dynamics: Basic Theory and Advanced Methods* (Cambridge University Press, Cambridge, England, 2009).
[31] See Supplemental Material at http://link.aps.org/supplemental/10.1103/PhysRevLett.119.056002 for details on the model systems, setup and validation of the computational approach, and the solvation structure of the H^+ and OH^- charge defects.
[32] J. Hutter *et al.*, CPMD program package, www.cpmd.org.
[33] J. P. Perdew, K. Burke, and M. Ernzerhof, Phys. Rev. Lett. **77**, 3865 (1996); **78**, 1396(E) (1997).
[34] D. Vanderbilt, Phys. Rev. B **41**, 7892 (1990).
[35] D. Marx, ChemPhysChem **7**, 1848 (2006); **8**, 209 (2007).
[36] S. Grimme, J. Antony, S. Ehrlich, and H. Krieg, J. Chem. Phys. **132**, 154104 (2010).
[37] D. Pan, L. Spanu, B. Harrison, D. A. Sverjensky, and G. Galli, Proc. Natl. Acad. Sci. U.S.A. **110**, 6646 (2013).
[38] M. Sharma, R. Resta, and R. Car, Phys. Rev. Lett. **98**, 247401 (2007).
[39] S. Grimme, J. Chem. Phys. **118**, 9095 (2003).
[40] F. Weigend, M. Häser, H. Patzelt, and R. Ahlrichs, Chem. Phys. Lett. **294**, 143 (1998).
[41] W. Wagner and A. Pruß, J. Phys. Chem. Ref. Data **31**, 387 (2002).
[42] M. Sprik, Faraday Discuss. **110**, 437 (1998).
[43] M. Sprik and G. Ciccotti, J. Chem. Phys. **109**, 7737 (1998).
[44] M. Sprik, Chem. Phys. **258**, 139 (2000).
[45] D. Marx, M. E. Tuckerman, and M. Parrinello, J. Phys. Condens. Matter **12**, A153 (2000).
[46] M. E. Tuckerman, A. Chandra, and D. Marx, Acc. Chem. Res. **39**, 151 (2006).
[47] M. E. Tuckerman, D. Marx, and M. Parrinello, Nature (London) **417**, 925 (2002).
[48] D. P. Fernández, A. R. H. Goodwin, E. W. Lemmon, J. M. H. Levelt Sengers, and R. C. Williams, J. Phys. Chem. Ref. Data **26**, 1125 (1997).
[49] A. V. Bandura and S. N. Lvov, J. Phys. Chem. Ref. Data **35**, 15 (2006).
[50] D. Marx, A. Chandra, and M. E. Tuckerman, Chem. Rev. **110**, 2174 (2010).
[51] N. Akiya and P. E. Savage, Chem. Rev. **102**, 2725 (2002).

[52] H. Weingärtner and E. U. Franck, Angew. Chem., Int. Ed. Engl. **44**, 2672 (2005).
[53] D. J. Bonthuis, S. Gekle, and R. R. Netz, Phys. Rev. Lett. **107**, 166102 (2011).
[54] D. J. Bonthuis, S. Gekle, and R. R. Netz, Langmuir **28**, 7679 (2012).
[55] Y. Wu, H. L. Tepper, and G. A. Voth, J. Chem. Phys. **124**, 024503 (2006).
[56] C. Schaaf and S. Gekle, Phys. Rev. E **92**, 032718 (2015).
[57] R. Renou, A. Szymczyk, G. Maurin, P. Malfreyt, and A. Ghoufi, J. Chem. Phys. **142**, 184706 (2015).